PRETRANSFORMATION PHENOMENA AND MARTENSITIC TRANSFORMATIONS IN TITANIUM NICKELIDE ALLOYS

V. G. Pushin, V. V. Kondrat'ev, and V. N. Khachin

UDC 669.295.24.539.370

INTRODUCTION

Many studies have been made of intermetallic compounds based on nearly equiatomic compositions of titanium nickelide (NiTi) and some of its ternary alloys (NiTiFe, NiTiCu, NiTiAl, NiTiAu, etc.). It has been established that they have such universal mechanical properties as shape memory pseudoelasticity, superelasticity, reversible form change, high damping capacity, fatigue resistance, and several others (see, e.g., [1, 2]).

As is known, complex structural transformations of the martensitic type are seen in these alloys at certain temperatures. According to the data from most investigators [1-11], the crystalline structure of the initial high-temperature phase is a bcc lattice ordered atomically according to the type CsCl(B2) with the unit cell parameter $a_0 = 0.3015$ nm. As concerns the crystalline structure of the martensite, it has not been so unambiguously determined and has been described by different authors as hexagonal [12], monoclinic (two types with parameters $a = 0.519$, $b = 0.496$ nm, $c = 0.425$ nm, and $\gamma = 99°$ and $a' = 0.519$ nm, $b' = 0.552$ nm, $c' = 0.425$ nm, $\tau' = 116°$) [13], monoclinically orthorhombically deformed (B19') with parameters $a = 0.2889$ nm, $b = 0.412$ nm, $c = 0.4622$ nm, and $\beta = 96.8°$ [5, 6, 14], triclinic (with parameters close to those in [6] but with angles $\alpha = 0.320$ nm, $b' = c' = 0.415$ nm, $\beta' = 91°$) in the form of alternating plates [16] or characterized by a set of long-period layered lattices with hexagonal and rhombohedral symmetry (4H, 2H, 3R, 12R, 18R) and certain sequences of ordered stacking faults [7]. We should also mention [3], which confirmed that the martensitic structure cannot be exactly determined because the magnitude and character of the shear displacements of the atoms which form it depend on temperature.

The martensite in ternary alloys based on NiTi (with Fe, Al, Cu) is of the monoclinic type B19' [8, 10, 17, 18]. It was also established that in alloys containing gold or copper in concentrations above a certain critical value the martensitic structure may change from monoclinic to orthorhombic ($\alpha = \beta = \gamma = 90°$) and only its subsequent cooling will produce an increasing monoclinic distortion [18].

The difficulties encountered in establishing the type of martensite are evidently due to its internal defectiveness: the presence of a large number of microtwins and stacking faults [6-8, 12], as well as several other structural features typical of NiTi alloys.

It has been found that in the region of temperatures and compositions preceding the point of beginning of formation of low-symmetry martensite M_S in NiTi alloys there are anomalies in several physical properties: the velocity of sound waves and the elastic constants [19], internal friction [2, 20-22], electrical resistivity [5, 10, 11, 15, 20-22], specific heat [24, 25], and others. These data provide evidence of a reduction in the stability of the crystalline lattice and, possibly, the generation of features in the electronic spectrum in the alloys in the pretransformational or premartensitic state. As the point M_S is approached one also sees various diffraction effects [3-11] (diffuse bands [3-5, 15, 22], extra reflections in certain reciprocal-lattice positions [4-11, 22], and several others). It should be noted that these effects have been seen not only by electron diffraction [4-8, 10, 11, 22], but also by x-ray diffraction [3, 5, 18, 22] and neutron diffraction [9]. The appearance of the diffuse bands has been explained as the result of scattering on acoustic vibrations of the crystalline lattice, which begins to lose stability in the premartensitic state [4, 5]. The observation of extra reflections 1/3 the distance between Bragg reflections of the type 110_{B2} was taken as proof by the authors of [3] that the

Institute of Metal Physics of the Ural Science Center of the Academy Sciences of the USSR and the Siberian Physicotechnical Institute at Tomsk University. Translated from Izvestiya Vysshikh Uchebnykh Zavedenii, Fizika, No. 5, pp. 5-20, May, 1985.

0038-5697/85/2805-0341$09.50

initial high-temperature phase also has a cubic superstructure which is more complexly ordered than B2 (the cubic superstructure has the space group P3m1) and has the parameter $a_0 = 0.9$ nm. Nagasawa [7] proposed a unit cell somewhat different from [3] to describe the cubic superstructure of the intermediate phase with $a_0 = 0.9$ nm. Finally, the same reflections of the type $\frac{1}{3}\langle 110\rangle$ were linked by the authors of [4] with piercings of the Ewald sphere at these positions of the reciprocal lattice (RL) by the above diffuse bands in certain directions ($\langle 2\bar{1}0\rangle$ and $\langle 321\rangle$), while in [5] they were linked with static waves of atomic displacements of the type $\{110\}\langle 1\bar{1}0\rangle$. In several studies, particularly [26], it was argued that reflections of the "1/3" type are due to the appearance of a ω-phase, which occurs widely in metastable alloys of titanium and zirconium [27].

According to data from x-ray and neutron diffraction studies [9, 15, 20], the Bragg peaks 110_{B2}, 111_{B2}, etc. undergo marked broadening before the martensitic transformation and then split. This provides grounds for suggesting, in accordance with [9], that there is an increase in rhombohedral distortion of the initial B2 phase. The authors of [7, 23] reason that in this case an intermediate rhombohedral phase with the parameters $a = 0.602$ nm and $\alpha = 90.7°$ [15] is formed. This was refined in [4] to $a = 0.903$ nm and $\alpha_{min} = 89.3°$.

Recent studies [10, 11] have reached conclusions regarding the formation of charge density waves (static modulations of conduction electrons [28]) and associated incommensurable static waves of atomic displacements on the basis mainly of electron microscope investigations of pretransformation phenomena in the alloy $Ti_{50}Ni_{47}Fe_3$ and the fact that extra reflections of the 1/3 type are shifted somewhat toward the nearest Bragg B2 reflections (by about 0.45% from the positions $\frac{1}{3}\langle 110\rangle$ and by about 1.2% from the positions $\frac{1}{3}\langle 112\rangle$) and thus are slightly incommensurable relative to the period of the initial phase.

Consequently, various anomalies of physicomechanical properties which are of practical importance have now been observed and studied in detail in NiTi alloys undergoing thermoelastic martensitic transformation. However, despite the large amount of empirical data available, there are serious disagreements regarding the sequence and mechanisms of the structural phase transformations in these alloys. Discussions so far have dealt with the crystal structure of the resulting martensite phases and the structure of the premartensitic state, as well as with the nature of their occurrence. Still unclear is the relationship between the structural and physical pretransformation phenomena on the one hand and the subsequent martensitic transformation on the other hand.

The present article reports on a comprehensive, systematic study of the structure and properties of NiTi alloys. A thermodynamic study is made of the stability of intermediate shear structures and their relationship to the intermediate R and final martensite phases using a model of static displacement waves. Analysis of structural data and the derivation of theoretical conclusions make it possible to establish the sequence of structural transformations in these alloys.

1. EXPERIMENTAL MATERIAL AND METHOD

The study was conducted by transmission electron microscopy and in situ electron microdiffraction on an IEM-150 electron microscope with an accelerating voltage of 150 kV (in the temperature range −150-+150°C), as well as by x-ray diffraction using a DRON-2 diffractometer equipped with low- and high-temperature attachments. We measured electrical resistance, frequency of torsional vibrations, and mechanical properties. Binary NiTi alloys containing 50.0, 49.0, and 48.7% Ti and ternary alloys containing 50% Ti, 1 and 2% Fe, and the rest Ni or 50% Ti, 5 and 10% Cu, and the rest Ni (at.%) were investigated. The alloys were made from titanium iodide, NO-grade nickel, carbonyl iron, and electrolytic copper by electric-arc refining in an atmosphere of purified helium. The ingots were rolled into plates. The heat treatment of the alloys included long annealing in a vacuum at 800°C with subsequent cooling with the furnace or quenching from 900°C in a 5% solution of KOH.

2. RESULTS OF EXPERIMENTS AND DISCUSSION OF RESULTS

Premartensitic States in NiTi

1. All of the alloys studied had a B2-type structure in the initial state. Together with Bragg structural and superstructural reflections, the electron microdiffraction patterns for the range 100-150°C exhibited regions of diffuse scattering (DS) in the form of bands directed through certain structural reflections (except for 000). The intensity of the DS, meanwhile, is somewhat greater near the reflections than between them (Figs. 1 and 2). Construction of the complete pattern of distribution of diffuse scattering in the reciprocal-lattice space showed that the DS regions are layers along {111} planes passing through points of the reciprocal lat-

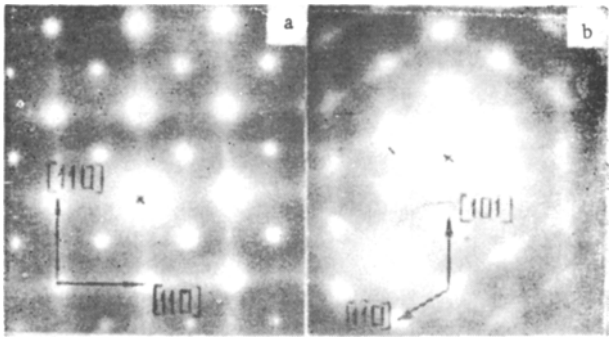

Fig. 1. Electron diffraction patterns of an Ni−49% Ti alloy corresponding to sections of the reciprocal lattice (RL) $(001)_{B2}$ (a) and $(111)_{B2}$ (b). Temperature of the observation T ≅ 100°C.

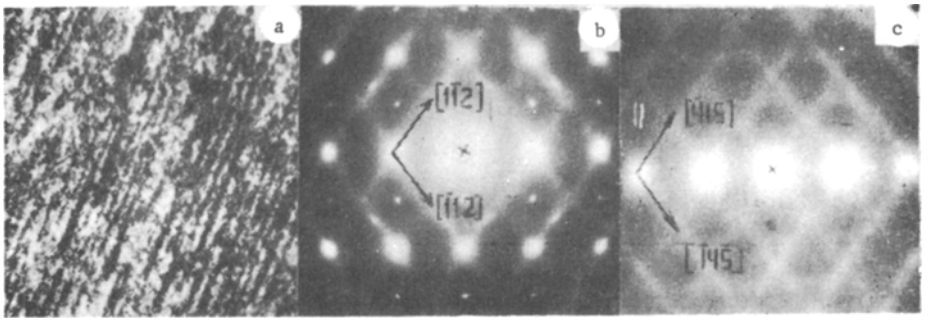

Fig. 2. Twinned martensite B19' (a − ×15,000) and electron diffraction patterns of the initial phase obtained at T ≅ 100°C (b − RL section $(110)_{B2}$, c − $(533)_{B2}$). Ni − 50% Ti−10% Cu alloy.

tice (RL). The intensity of scattering in these layers is unevenly distributed and changes regularly in relation to the position in the RL space. Scattering is absent when the RL vector **g** is directed parallel to the {111} plane (thus "extinguishing" the DS in planes passing through the center of the RL). The most intense diffuse bands are located along the ⟨110⟩ and ⟨112⟩ directions of the RL. The scattering is also characterized by the fact that when the vector **g** increases (i.e., when the angle of reflection 2θ increases), DS remains fairly intense compared to the markedly weaker Bragg reflections. With a decrease in temperature below 150°C, DS in all of the investigated alloys increases. Comparison of DS in the different alloys showed that DS is somewhat more intense in the binary NiTi alloys and ternary NiTiFe alloys than in the NiTiCu alloys.

Characteristic features of the DS observed − its periodicity and the regular extinction and intensification of scattering − make it possible to link DS with waves of atomic displacements which distort the ideal crystalline lattice [27]. In this case, the intensity of DS at points removed from the nearest points of the RL hk*l* by the vector **k** is determined as [29]

$$I_{DS} \sim |A_\kappa (e_\kappa \cdot g)|^2, \quad (1)$$

where A_k and e_k are the amplitude and polarization vector of a displacement wave with the wave vectors $k = g - H_{hkl}$; H_{hkl} is the vector of the point of the RL. Thus, analysis of the complete pattern of DS distribution makes it possible to construct spectra of atomic displacement waves after we have determined the regions of the wave vectors **k** and the directions of polarization e_k of the displacement waves with maximum amplitudes in the reciprocal space (in its unit cell relative to the point 000, coincident with the first Brillouin zone of the **k**-space) (Fig. 3).

The extended DS between the reflections located on the {111} planes of the RL is due to the shortwave part of the vibration spectrum of the atoms and according to [30] may be connected with shuffle displacement of dense-packed chains of atoms along ⟨111⟩ in bcc crystals, the atoms in the chains vibrating relative to each other as a unit whole. With a decrease in temperature, an increase in the displacements of these chains (they

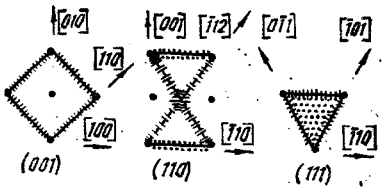

Fig. 3. Schematic representation of the spectrum of displacement waves in the form of plane sections of the k-space. The arrows and dots denote directions of the displacement-wave polarization vectors in the regions of the wave vectors with maximum amplitude.

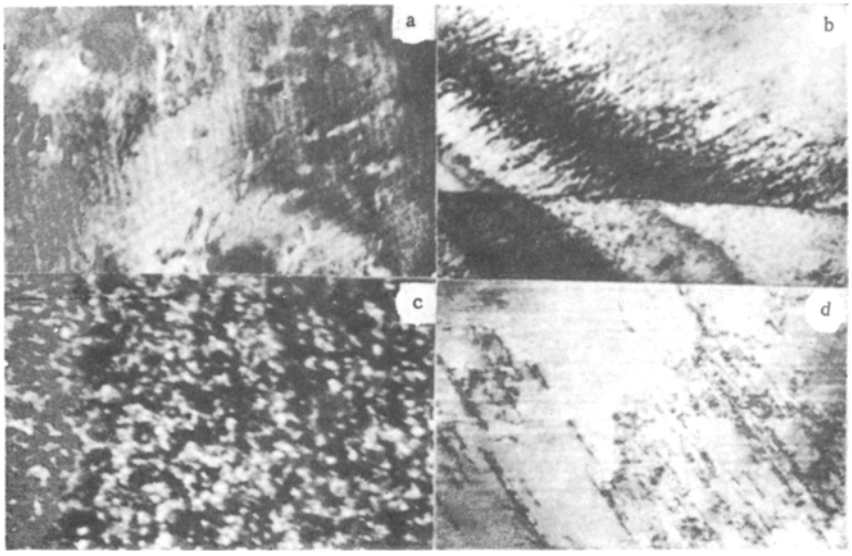

Fig. 4. Banded contrast and contrast from microdomains with ISS. a) T = 100°, b) T = 20°, c) T = 10°, d) T = 50° (after removal cycling), ×50,000.

being unusual line defects in the crystal) and the anharmonic nature of the lattice result in increasing correlation in the motion of the chains along dense-packed planes $\{110\}$ and $\{112\}$. The latter is expressed in reinforcement of DS in the directions $\langle 110\rangle$ and $\langle 112\rangle$ of the RL. The correlation of the atomic displacements in the planes is greater than the correlation of the planes relative to each other. This accounts for the continuous character of scattering in bands along $\langle 110\rangle$ and $\langle 112\rangle$.

As in [4-6, 8, 10], electron microscope bright-field images, especially near extinction contours, show contrast in the form of undulations. The intensity of the latter increases and the banding of the contrast is reinforced with a decrease in temperature (Fig. 4a). Dark-field images obtained in bands along $\langle 110\rangle$ and $\langle 112\rangle$ of the RL show local "luminous" regions ($\lesssim 3$ nm in size at 100°C). The nature of the diffractive contrast and the diffuse scattering seen with a decrease in temperature are connected with an increase in atomic displacements localized in microregions in which the structure and symmetry are already altered from the structure and symmetry of the initial matrix. Such a premartensitic state, as in other metastable alloys [27], is related to the short-range order of the atomic displacements (DSO) [22]. The internal structure of the submicrodomains with DSO will be determined by the superposition of shortwave atomic displacements mainly of the type $\{110\}\langle 1\bar{1}0\rangle$ and $\{112\}\langle 11\bar{1}\rangle$, localized within the domains. Their spatial arrangement and the character of coupling with the surrounding matrix, dependent on the elastic anisotropy parameter of the cubic crystal $A = c_{44}/c'$, determine the longwave modulation of the displacements and, accordingly, the form of DS near the Bragg reflections.

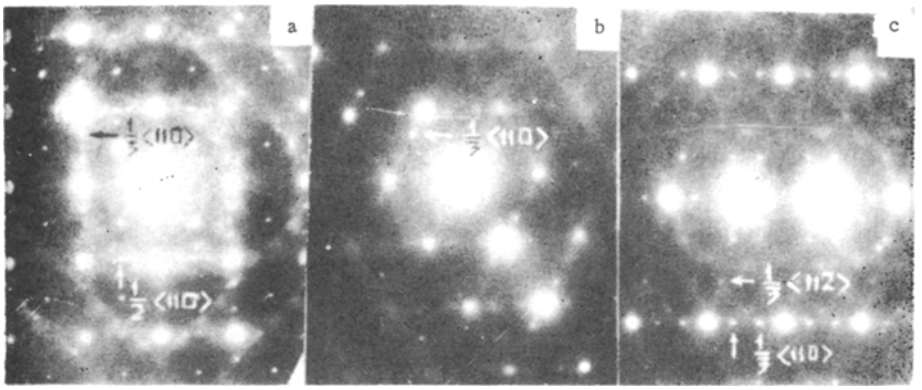

Fig. 5. Electron diffraction patterns of alloys Ni−49.0% Ti (a, b) and Ni−50% Ti−2% Fe (c) corresponding to RL sections $(001)_{B2}$ (a), $(111)_{B2}$ (b), $(113)_{B2}$ (c). The temperature of the observation was close to 20°C.

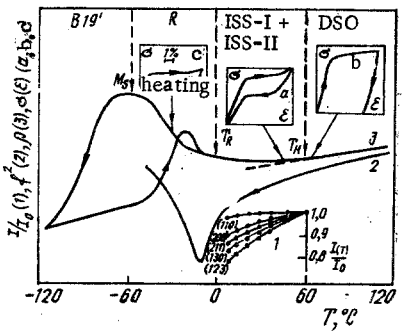

Fig. 6. Curves of the temperature dependence of the relative intensity of Bragg reflections $I(T)/I_0$ (T = 60°C) (1), the square of the frequency of vibration f^2 (2), electrical resistivity ρ (3), and curves of the dependence of the stress σ on the strain ε at different temperatures (a, b, c) for an Ni − 49.0% Ti alloy annealed at 800°C for 1 h.

2. When the alloys are cooled below a certain temperature T_n, which is different for different alloys, diffuse extra reflections (or satellites) appear and are reinforced on diffuse bands along $\langle 110\rangle$ and $\langle 112\rangle$ of the RL. These reflections are described by the wave vectors $k_n \approx {}^1/_3\langle 110\rangle^*$, $\sim {}^1/_3\langle 112\rangle$. Extra reflections with $k_n \approx {}^1/_2\langle 110\rangle$ are subsequently formed (Fig. 5). Here, as in [5], electron diffraction shows a reduction in the intensity of the continuous regions of DS, while x-ray diffraction shows a reduction in the intensity of the Bragg reflections (Fig. 6) [22]. It should be noted that the authors of [31] also observed reversible hysteresis-free broadening of the 110_{B2} line near M_S. The extra reflections, as the continuous DS, are regularly extinguished in the RL space and can be attributed (in accordance with (1) with the development of crystallographically ordered cross-polarized plane displacements of atoms with wave vectors and polarizations of the form $\sim {}^1/_3\langle 110\rangle_k$, $\langle 1\bar{1}0\rangle_{e_k}$, $\sim {}^1/_3\langle 112\rangle_k$, $\langle 11\bar{1}\rangle_{e_k}$, $\sim {}^1/_2\langle 110\rangle_k$, $\langle 1\bar{1}0\rangle_{e_k}$. Extra reflections of the type $\sim {}^1/_2\langle 100\rangle$ of the RL were also sometimes visible. These reflections could be described by longitudinally polarized atomic-displacement waves of the type $\sim {}^1/_2\langle 100\rangle_k$, $\langle 100\rangle_{e_k}$ [32].

It should be noted that the extra reflections $\sim {}^1/_3\langle 110\rangle$ and $\sim {}^1/_3\langle 112\rangle$ are shifted somewhat toward the nearest Bragg reflections from positions which are multiples of three, while extra reflections of the type $\sim {}^1/_2\langle 110\rangle$ are extended along $\langle 110\rangle$ of the RL to both sides from the "1/2" positions (Fig. 5). This agrees with the data in [5, 9, 11, 22]. As before, intense regions of DS are seen near the reflections of the B2 phase, these regions characterizing the spectrum of anisotropic longwave distortions of the crystalline lattice of the matrix.

*We did not see these satellites in the NiTiCu alloys.

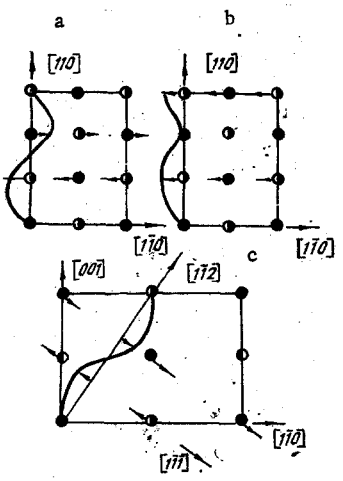

Fig. 7. Diagrams of periodic shuffle displacements of atoms leading to the appearance of satellites of the type $\frac{1}{3}\langle 110\rangle$ (a), $\frac{1}{2}\langle 110\rangle$ (b), $\frac{1}{3}\langle 112\rangle$ (c).

The electron microscope studies showed that contrast of the undulatory type becomes especially intense at the "satellite" stage (Fig. 4b). Microdomains of certain (corresponding to the given satellite k_n) variants "shine" on dark-field images in extra reflections of the types "1/3" and "1/2." The dimensions of these microdomains reach 10-30 nm at temperatures near room temperature (Fig. 4c). The data obtained shows that alloys at the satellite stage in the premartensite state are characterized by a distribution of microdomains in the initial matrix. The internal structure of these microdomains is described by periodic atomic displacements (a displacement wave) of the following type

$$u^{(i)}(R) = \sum_n A_n^{(i)} e(\kappa_n^{(i)}, j_n) \sin(\kappa_n^{(i)} R + \delta_n^{(i)}), \qquad (2)$$

where $A_n \equiv A\kappa_n$, j_n, $\delta_n^{(i)}$ are the amplitude and the number of the branch and the phase of the n-th displacement wave from the positions R of the initial phase (in the i-th domain).

Disturbance of the correlation between the periodic displacements of the planes along and across the direction of displacement-wave propagation (change in the phase $\delta_n^{(i)}$) leads to errors in stacking of the shear planes (antiphase domain boundaries of different types). In constructing a realistic model of the structure, one should consider the presence of several crystallographically equivalent directions of atomic displacements $<\kappa_n^{(i)}>$, $<e(\kappa_n^{(i)}, j_n)>$ and the possibility of their interference, as well as the presence of displacement waves of different periodicity ($|k_n| = 2\pi/\lambda$, λ is the wavelength). It is important to emphasize that these features of the fine structure, even with a length of the wave vector k_n equal to a rational fraction of the RL vector, lead to shifting or blurring (depending on the form of k_n) of the DS maximums in incommensurable positions. Finally, the local nature of the microdomains of the displaced atoms also causes broadening (diffuseness) of the extra reflections.

Detailed electron microscope study of the structure of the premartensite state of an Ni–49.5% Ti alloy by the method of stereoscopic images $2\frac{1}{2}$D [32] made it possible to distinguish two different types of ensembles of microdomains forming extra reflections of the type $\frac{1}{3}\langle 110\rangle$ and $\frac{1}{2}\langle 110\rangle$, with mean dimensions of 20 and 5 nm, respectively. In the same work, the authors, employing direct resolution of the crystalline lattice, observed the internal structure of the microdomains as being fully coherent with the undistorted matrix. They also detected antiphase domain boundaries of different types.

Thus, analysis of the available experimental data enables one to explain the basic features of observed diffraction effects and the fine structure of alloys at the "satellite" stage, having recognized it as an independent structural state replacing the DSO and characterized by localized intermediate shear structures (ISS): ISS-I, leading to the appearance of extra reflections of the type "1/3"; ISS-II, with extra reflections of the type "1/2." Figure 7 diagrams shortwave shuffle displacements of both types. Since all crystallographically equivalent variants of microdomains exist with ISS's distributed randomly over the volume of the matrix, the structure of the alloys retains its cubic symmetry on the average.

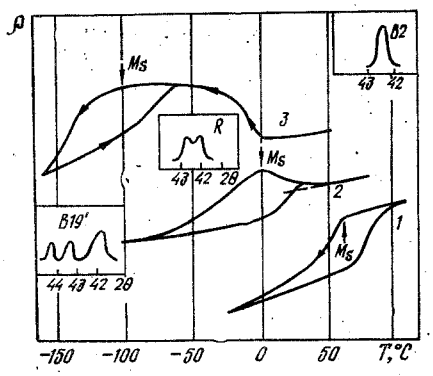

Fig. 8. Curves of the temperature dependences of the electrical resistivity of alloys Ni – 50% Ti (1), Ni – 49.5% Ti (2), and Ni – 50% Ti – 3% Fe (3) and profiles of the x-ray lines of the alloys in the initial state (B2) and after the formation of R-martensite and B19' martensite.

3. The properties of NiTi alloys are anomalous in the structural state with DSO and ISS. Initially a decrease in temperature is accompanied by a decrease in the natural frequency of vibration of the specimens $f^2 \sim G$ (G is the shear modulus), $dG/dT > 0$ (curve 2 in Fig. 6).

Measurements of the temperature dependences of the elastic constants, first made on single crystals of NiTi in [19], showed that as M_S is approached all of the elastic constants c_{11}, c_{44}, and c' decrease simultaneously. The value of c_{44} decreases more than that of c', so that the parameter A remains small (decreasing from 2.18 to 1.90 in the temperature range from 40 to 5°C). More detailed data obtained by the authors recently* on TiNi single crystals and alloys showed that each structural state (B2, BSO, ISS, and the R and B19 phases) corresponds to a unique regular behavior of the moduli c_{44} and c' and the parameter A. In particular, the transition from DSO to ISS and then to the R (or B19') phase is accompanied by a gradual increase in softening of c_{44} beginning at the point T_n and reaching a maximum at the moment MP (T_R). Softening of the modulus c' is slight and it diminishes as a result of the parameter A, reaching anomalously low values below T_R. In other words, before MP the initial lattice exhibits a definite tendency toward a decrease in elastic anisotropy in the simultaneous presence of several soft shear systems. It is this very situation that raises the possibility of occurrence of a whole system of atomic displacement waves in the pretransformation region and almost simultaneous opening of two different MP channels.

Comparison of data from measurement of electrical resistivity as a function of temperature on the one hand and structural observations on the other hand makes it possible to conclude that at the ISS stage the curve of electrical resistivity (ρ) vs temperature begins to deviate from linearity, i.e., $d\rho/dT$ decreases and then changes sign [22] (Fig. 6). The exception is the equiatomic NiTi alloy, for which these features of resistivity are manifest only after thermal cycling [5, 20] and evidently reinforce the pretransformation phenomena but on the other hand stabilize the alloy in regard to martensitic transformation as a result of phase work hardening [20]. Electrical resistivity anomalies are also absent in NiTiCu alloys [33, 34]. Figure 8 shows three different temperature dependences $\rho(T)$ typical of titanium nickelide alloys. It should be emphasized that the changes in the structure and properties of the alloys in the premartensitic state (DSO and ISS) occur continuously and are completely reversible with thermal cycling.

At the stage of formation of incommensurable ISS's (below T_n), an external load can easily initiate martensitic transformation and induce superelasticity (Fig. 6). At temperatures above T_n, no martensitic transformation occurs under load up to the yield point. The occurrence of a martensitic transformation at loads in excess of the yield point (i.e., with strictly plastic deformation of the alloys) increases deformability and induces superplasticity in NiTi alloys as seen in [21]. Considering that the anomalous behavior of the shear modulus and plastic strain begin at 400-550°C for different alloys, these temperatures can be taken as the points of beginning of reduction in the stability of the crystalline lattice and formation of the premartensitic state with DSO.

*The empirical results were obtained by S. A. Muslov and will be published as a separate report.

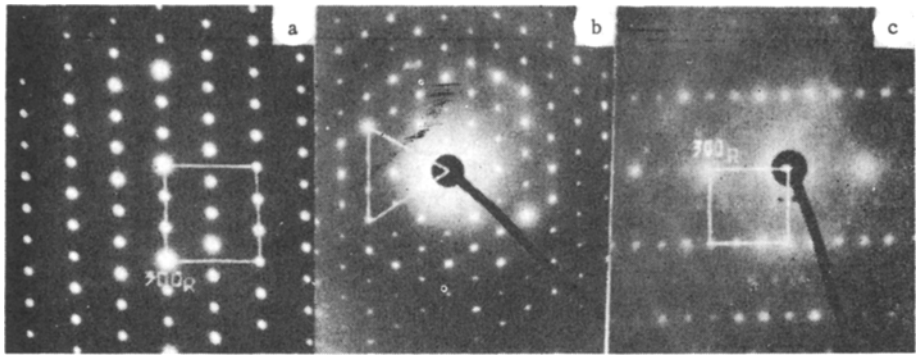

Fig. 9. Electron diffraction patterns of R-martensites of alloys Ni–49.0% Ti (a, b) and Ni–50% Ti–2% Fe (c) corresponding to the axes of zones of reflecting planes $[011]_R$ (a, c) and $[001]_R$ (b). Observation temperature near 20°C.

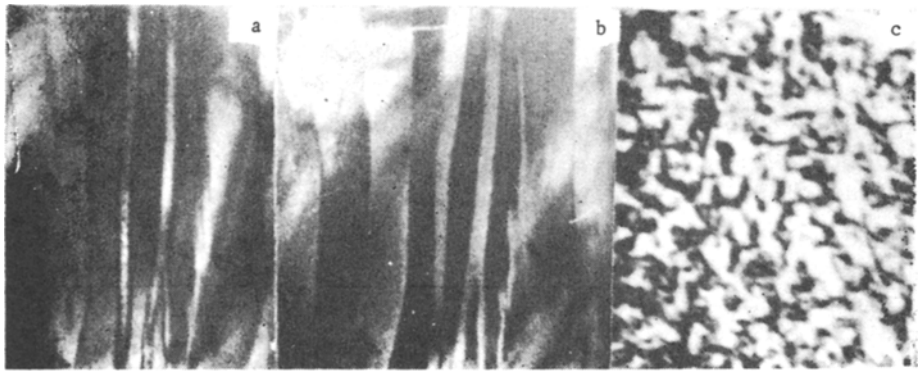

Fig. 10. Microstructure of alloys in the state of R-martensite (a, b – ×5000); c – dark-field image of antiphase domains in the 200_R reflection, ×100,000.

First Martensitic B2 → R Transformation

With cooling of NiTi and NiTiFe alloys to a certain critical temperature T_R (below room temperature for nonequiatomic binary alloys and ternary NiTiFe alloys), electron diffraction patterns show intensification of a certain variant of extra reflections and their shift to strictly commensurable "1/3" positions along three ⟨110⟩ directions of the RL perpendicular to one of the four ⟨111⟩ directions of the RL. Also the "1/3" reflections located in the RL planes passing through the RL origin are no longer extinguished (Fig. 9). At this moment, domains with ISS's undergoing continuous growth during cooling cease their "joining," and lamellar crystals of R martensite of macroscopic dimensions are formed (Fig. 10). Analysis of light- and dark-field images of the R martensite shows that its individual crystals contain antiphase domain boundaries (Fig. 10c) (see [11] also). The formation of antiphase domain boundaries (ADB) occurs on the boundaries of adjacent ISS domains of a certain type during their self-consistent restructuring in the course of the martensite transformation.

Broadening is seen on x-ray diffraction patterns below T_R. This is following by "resolution of the splitting" of several Bragg reflections formerly 110_{B2}, 112_{B2}, and 222_{B2}, which is evidence of rhombohedral distortion of the crystalline lattice of martensite (Fig. 8) [15, 20, 18]. The microdiffraction patterns already no longer have cubic symmetry (Fig. 9) and were indexed in a hexagonal basal plane with the axes $a_R^* \approx a_{B2}^*/3$ $[\bar{1}10]$; $b_R^* \approx a_{B2}^*/3$ $[\bar{1}01]$; $c_R^* \approx a_{B2}^*/3$ [111], which corresponds to a hexagonal unit cell with the periods $a_R \approx a_{B2}$ $[\bar{1}2\bar{1}] \equiv a_{B2}\sqrt{6}$; $b_R \approx a_{B2}$ $[\bar{1}\bar{1}2] \equiv a_{B2}\sqrt{6}$; $c_R \approx a_{B2}$ $[111] \equiv a_{B2}\sqrt{3}$ [22] . Since there are four equivalent ⟨111⟩ directions in the cubic crystal along one of which uniform expansion occurs with rhombohedral distortion during the B2 → R transformation, four variants of lamellar R-phase domains are formed. These domains are twinned relative to each other along the {110} twinning planes. This transformation can be classified as an "incommen-

surable phase – commensurable phase" transformation [11]. There is every reason to believe that the ISS-I intermediate shear structure, accounting for the appearance of incommensurable reflections of the "1/3" type, are a precursor of the first martensite transformation, while microdomains with ISS-I play the role of centers of R-martensite nucleation. Meanwhile, individual R-crystals are formed by the gradual joining of many growing nuclei (i.e., by the multiple-nucleus mechanism). The restructuring of domains with ISS-I into the R phase will be examined analytically in the next section.

Experiments with thermal cycling showed a high degree of reversibility of the transformation B2 $\rightleftharpoons$ R and almost complete recovery of the form, location, and orientation of the R-martensite crystals after the transformation cycles (compare a and b in Fig. 10). Except for ADB in the martensite and microdomains with ISS in B2 austenite, no structural defects were seen during B2 $\rightleftharpoons$ R cycling. Near T_R there is a sharp increase in electrical resistivity, a shear modulus minimum, and a plastic strain maximum [20-22]. All of these findings indicate that rhombohedral (trigonal) R martensite is formed at T_R.

The B2 $\rightarrow$ R transformation is accompanied under stress by macroscopic shape deformation and shape memory phenomena [23]. Below T_R, an external load easily induces a second martensite transformation and, accordingly, the phenomenon of superelasticity [22]. The stage of strain accumulation and recovery is characterized by a distinctly two-stage nature due to two processes: monodominization of existing R martensite, and the formation and subsequent monodominization of low-symmetry martensite.

Second Martensitic B2(R) $\rightarrow$ B19' Transformation

A reduction in temperature below M_S (down to −150°C) leads to a second martensitic transformation. This involves the formation of plate crystals internally twinned along $(11\bar{1})_{B19'}$ (Fig. 11). Study of their crystallographic relationship with R martensite and B2 austenite made it possible to establish the following orientation relations:

$$(111)_{B2} \parallel (001)_R \parallel (110)_{B19'};\ (\bar{1}10)_{B2} \parallel (100)_R \parallel (001)_{B19'}.$$

The presence of fine DS lines along $[001]_{B19'}$ on the electron diffraction patterns of B19' martensite (Fig. 11c) is evidence of the formation of random stacking faults along $(001)_{B19'}$ inside the martensite crystals. It is also interesting that the extra reflections $k \approx \frac{1}{2}\langle 110\rangle$ seen in the premartensitic state and referred in this article to ISS-II coincide in position with certain reflections from martensite with the B19' structure. Crystallographic examination of the restructuring of the lattices B2 $\rightarrow$ B19', taking into account the formation of domains with ISS-II during its first stage, confirm their important role in the formation of monoclinic (orthorhombic) martensite (Fig. 12). It can be concluded on the basis of the data obtained that ISS-II microdomains precede and are causally linked with low-symmetry martensite in NiTi. It should be noted that stacking faults along $(001)_{B19'}$ turn out to be parallel to the shuffle planes in the ISS-II domains, providing additional evidence of the validity of the restructuring scheme depicted in Fig. 12.

Cycling of the transformations B2(R) $\rightleftharpoons$ B19', in contrast to B2 $\rightleftharpoons$ R, leads to marked accumulation of dislocations of a certain type (loop, dipole, planar pile-ups) in the austenite. These dislocations are seen against a background of banded contrast (Fig. 4d). The formation of B19' martensite with the application of an external load is also connected with the accumulation of macroscopic strain and shape memory phenomena during subsequent heating.

The established principles of structural changes and the physicomechanical properties of NiTi alloys are general in character. There are some differences, such as for the critical transformation temperatures (T_n, T_R, M_S): high-nickel binary alloys are characterized by a broad range of existence of incommensurable ISS's ($\Delta T = T_n - T_R$ is about 60°C after annealing and about 120°C after quenching). This range contracts toward T_R in NiTiFe alloys. A feature of NiTiCu alloys is the absence of satellites of the $\frac{1}{3}\langle 110\rangle$ type, the B2 $\rightarrow$ R martensitic transformation, and electrical resistivity anomalies.

3. THERMODYNAMIC ANALYSIS OF THE STABILITY OF PREMARTENSITIC STATES

1. We will examine the thermodynamic stability of the crystalline lattice of an NiTi alloys relative to the atomic displacements leading to the formation of ISS-I. As already noted, this structure corresponds to extra reflections of the 1/3 type on electron diffraction patterns and is described in the representation of fluctuational atomic displacements by two types of transverse lattice waves with wave vectors and polarization vectors:

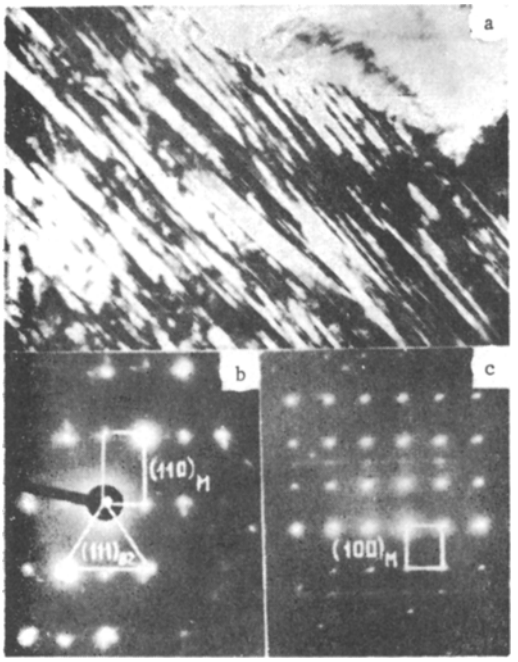

Fig. 11. Twinned B19' martensite of NiTi alloys, T = −60°, ×2000 (a), and electron diffraction patterns of martensite (b, c).

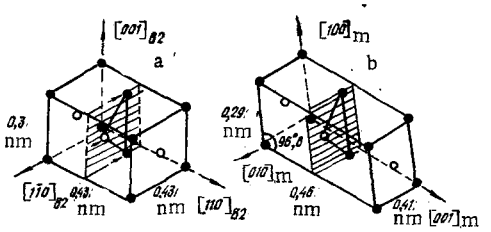

Fig. 12. Restructuring scheme B2 − B19' for the first stage of ISS-II formation (a), and for the second stage, in which uniform deformation of the elementary unit cell of the B2 distortion phase takes place, leading to formation of the monoclinic unit cell of B19' martensite (b).

$$\kappa = 1/3\ \langle 110\rangle,\ e_\kappa \parallel \langle 1\bar{1}0\rangle;\ \kappa = 1/3\ \langle 112\rangle,\ e_\kappa \parallel \langle 11\bar{1}\rangle. \tag{3}$$

It follows from the existence of such waves with a change in temperature and concentration that ISS's of complex form may occur in NiTi and NiTiFe alloys near M_S. These ISS's are described in the model of static displacement waves in [35] by a superposition of waves (2). Considering this, to within the terms A_1^4 we can write the following for the expression for the free energy of an anharmonic crystal [35]:

$$\begin{aligned} F = \frac{N}{4}\Bigg(\overline{m}\sum_n \Omega_n^2 A_n^2 + \frac{1}{3!}\sum_{n,n',n''} U(\kappa_n j_n, \kappa_{n'}\ j_{n'}, \kappa_{n''} j_{n''}) \times \\ \times \Delta(\kappa_n + \kappa_{n'} + \kappa_{n''}) \cos(\delta_n + \delta_{n'} + \delta_{n''}) A_n A_{n'} A_{n''} + \\ + \frac{1}{4!}\sum_{n,n',n'',n'''} U(\kappa_n j_n, \ldots \kappa_{n'''} j_{n'''}) \Delta(\kappa_n + \ldots + \kappa_{n'''}) \times \\ \times \cos(\delta_n + \ldots + \delta_{n'''}) A_n A_{n'} A_{n''} A_{n'''}. \end{aligned} \tag{4}$$

Here

$$\Omega_n^2 \equiv \Omega^2(\kappa_n j_n) = \frac{1}{m}\sum_h U_{0h}^{\alpha\beta} e_{\kappa_n j_n}^{\alpha} e_{\kappa_n j_n}^{\beta} e^{i\kappa_n h} \tag{5}$$

are the frequencies of vibration of the atoms in the initial phase; N is the number of atoms in a unit volume; $\bar{m}$ is the "mean" mass of an atom of the alloy; $U_{0h}^{\alpha\beta}$ are second-order mechanical constants,

$$\begin{aligned} U(\kappa_1 j_1, \kappa_2 j_2, \kappa_3 j_3) &= \mathrm{Im}\Big(\sum_{h,h'} U_{0hh'}^{\alpha\beta\gamma} e_{\kappa_1 j_1}^{\alpha} e_{\kappa_2 j_2}^{\beta} e_{\kappa_3 j_3}^{\gamma} e^{i(\kappa_1 h + \kappa_2 h')}, \\ U(\kappa_1 j_1, \ldots \kappa_4 j_4) &= \sum_{h,h',h''} U_{0hh'h''}^{\alpha\beta\gamma\delta} e_{\kappa_1 j_1}^{\alpha} \cdot \ldots \cdot e_{\kappa_4 j_4}^{\delta} e^{i(\kappa_1 h + \ldots + \kappa_4 h'')} \end{aligned} \tag{6}$$

are Fourier images of the mechanical constants of the third and fourth orders $U_{0hh'}^{\alpha\beta\gamma}$ and $U_{0hh'h''}^{\alpha\beta\gamma\delta}$; h is the radius vector of the equilibrium position of the atoms relative to the zero point; $\Delta(\sum_n \kappa_n) = 1$ if $\sum_n \kappa_n$ is equal to zero or any RL vector, while $\Delta(\sum_n \kappa_n) = 0$ in the opposite case.

In deriving (4) we ignored the ordering of the atoms and actually examined a bcc lattice of "averaged" atoms with a mass $\bar{m}$ interacting with one another by means of "averaged" forces. This approximation can be used because the ordering temperature is considerably greater than M_S and the wave vectors of the characteristic vibration frequencies of the atoms are far from the boundary of the Brillouin zone. There is presently no data on the phonon spectra in NiTi, but pseudopotential calculations for β-brass with a B2-lattice [36] indicate that the phonon dispersion law is slightly dependent on the degree of long-range order and composition.

For nonequivalent waves (3) and a single crystallographic variant it is possible to uniquely select three waves such that we satisfy the condition $\Delta(\mathbf{k}_1 + \mathbf{k}_2 + \mathbf{k}_3) = 1$:

$$\begin{aligned} \kappa_1 = 1/3\ [11\bar{2}],\ e_1 = 1/\sqrt{3}\ [111];\ \kappa_2 = 1/3\ [\bar{1}01],\ e_2 = 1/\sqrt{2}\ [101]; \\ \kappa_3 = 1/3\ [0\bar{1}1],\ e_3 = 1/\sqrt{2}\ [011]. \end{aligned} \tag{7}$$

In this case, there is an interaction between waves (7) due to third-order anharmonism, which under certain conditions leads to a decrease in free energy (4).

With allowance for (7), Eq. (4) takes the form (for simplicity in the analysis, we will use the following simplifications: $A_2 = A_3$, and all of the parameters $U(k_1 j_1, \ldots, k_4 j_4)$ are equal to one another)

$$F = \frac{N}{4}\left[\bar{m}(\Omega_1^2 A_1^2 + 2\Omega_2^2 A_2^2) - \frac{1}{3!}U_{31}A_1^3 - \frac{1}{3}(U_{32} + U_{33})A_2^3 - U_3 A_1 A_2^2 + \frac{1}{16}U_4(A_1^4 + 6A_2^4 + 8A_1^2 A_2^2)\right], \tag{8}$$

where we have introduced the notation:

$$\begin{aligned} U_{3n} &= U(\kappa_n j_n, \kappa_n j_n, \kappa_n j_n)\cos(3\delta_n); \\ U_4 &= U(\kappa_n j_n, -\kappa_n j_n, \kappa_n j_n, -\kappa_n j_n = U(\kappa_n j_n, -\kappa_n j_n, \kappa_m j_m, -\kappa_m j_m). \end{aligned} \tag{9}$$

Using the method developed in [37], in a longwave approximation we can express the frequencies (5) and the third-order anharmonism parameters (9) through elastic moduli of the second c_{ij} and third c_{jik} order

$$\Omega_1^2 = \frac{3a}{2\bar{m}}(2c' + c_{44}),\ \Omega_2^2 = \frac{3a}{\bar{m}}c'; \tag{10}$$

where a is a lattice parameter,

$$\begin{aligned} U_{31} &= -\frac{1}{2}(9c_{11} + 17c_{44} + 28c_{12} - |c_{111} + 5c_{112}|)\cos(3\delta_1); \\ U_{32} &= \left(\frac{3}{2}\right)^{3/2}[|c_{111} - c_{112}| + 4(c_{44} + c' - c_{11})]\cos(3\delta_2); \\ U_3 &= \frac{3}{4}(|c_{111} + c_{112}| + 3c_{44} - 5c_{11})\cos(\delta_1 + \delta_2 + \delta_3). \end{aligned} \tag{11}$$

We will assume that $A_n > 0$. Then free energy (8) decreases under the conditions U_3, $U_{3n} > 0$. Knowing the elastic moduli c_{ij} and c_{ijk}, we can use Eq. (11) to determine the phases of the waves. The moduli c_{ij} for NiTi near M_S are known [19]: $c_{11} = 1.6 \cdot 10^{11}$ Pa, $c_{44} = 0.35 \cdot 10^{11}$ Pa, $c' = 0.17 \cdot 10^{11}$ Pa. As regards c_{ijk}, we assume that $c_{111} \simeq 10^{12}$ Pa and that $c_{112} = 1/2c_{111}$. The moduli c_{ijk} have such an order of magnitude in many investigated alloys with a B2 lattice [38]. There are two different choices of phases δ_n so that wave system (7) leads to a commensurable intermediate structure and the interaction of the waves decreases the energy (8) ($\delta_1 + \delta_2 + \delta_3 = 2\pi s$, $s = 0, \pm 1, \pm 2, \ldots$). In the first case: $\delta_n = 0$; in the second case, in which the wave $(\mathbf{k}_1, \mathbf{e}_1)$ prescribes ω-similar atomic displacements, $\delta_1 = \pi$, $\delta_2 = 0$, $\delta_3 = \pi$. Other equivalent values of the phases δ_n are possible and describe different ISS-1 antiphase domains.

The atomic displacement function for these two cases (the top sign corresponds to the first structure, which we will designate as ISS-I'; the bottom sign corresponds to ISS-I") can be written in the form

$$u(R) = \pm A_1 e_1 \sin\frac{2\pi}{3a}(R_x + R_y - 2R_z) + A_2\left[e_2 \sin\frac{2\pi}{3a}(R_z - R_x) \pm e_3 \sin\frac{2\pi}{3a}(R_z - R_y)\right]. \quad (12)$$

With allowance for ordering of the atoms, the resulting structure can be described in hexagonal coordinates with translational elements coinciding with the parameters of a unit cell of R martensite found in structural studies. The structure will contain 18 atoms in a cell. The subsequent ISS-I → R transformation evidently occurs as a result of uniform rhombohedral distortion of the ISS-I unit cell (with tension along $c = a$ [111]).

The structures ISS-I' and ISS-I" differ in the arrangement of the atoms inside the unit cell and are described by different free-energy expressions (8). The conditions under which these structures are metastable can be found by minimizing the free energy with respect to the amplitudes A_1 and A_2:

$$\frac{\partial F}{\partial A_1} = \frac{\partial F}{\partial A_2} = 0. \quad (13)$$

For ISS-I', this condition has the form

$$\overline{m}\Omega_2^2\left(1 - \frac{2}{3}U_3^2\overline{m}^{-1}\Omega_1^{-2}U_4^{-1}\right) < U_{32}^2(6U_4)^{-1}. \quad (14)$$

For ISS-I" to exist, it is necessary that

$$\left(2\overline{m}\Omega_1^2 - \frac{8}{3}\overline{m}\Omega_2^2\right) < \frac{4}{3}U_3^2U_4^{-1}. \quad (15)$$

Considering (10) and taking into account that $U_{32} \ll U_3$, we can express inequalities (15) and (14) through the elastic moduli and write them as follows:

$$(2c' + c_{44}) < \frac{4}{3}\eta' U_{32} \quad (\text{ISS-I'}), \quad (16)$$

$$14c' + c_{44} < \frac{4}{3}\eta'' U_3 \quad (\text{ISS-I"}), \quad (17)$$

where $\eta' = (1/3a)(U_{32}/U_4)$; $\eta'' = (1/3a)(U_3/U_4)$ are dimensionless theoretical parameters characterizing the relative atomic displacements in the new equilibrium positions.

Analysis of conditions (16) and (17) shows that ISS-I', being the result of instability of the wave $(\mathbf{k}_1\mathbf{e}_1)$ of ω-like atomic displacements relative to the two transverse waves $(\mathbf{k}_2\mathbf{e}_2)$ and $(\mathbf{k}_3\mathbf{e}_3)$, turns out to be thermodynamically more favorable than ISS-I".

Let us compare inequality (17) with the conditions of metastability of ω and 9R of the intermediate structures, which follow from minimization of the free energy

$$F_n = \frac{N}{4}\left(\overline{m}\Omega_n^2A_n^2 = \frac{1}{3!}U_{3n}A_n^3 + \frac{1}{16}U_4A_n^4\right) \quad (18)$$

and have the form [37]:

$$2c' + c_{44} < \frac{1}{4}\eta_\omega U_{31}, \eta_\omega = \frac{U_{31}}{3aU_4} (\beta \to \omega); \tag{19}$$

$$c' < \frac{1}{8}\eta_{9R} U_{32}, \ \eta_{9R} = \frac{U_{32}}{3aU_4} (\beta \to 9R). \tag{20}$$

Comparison of inequalities (17) and conditions (19)-(20) shows that ISS-I is thermodynamically more favorable than the ω-phase if

$$\frac{14+A}{2+A} < \frac{16}{3}\left(\frac{U_3}{U_{31}}\right)^2, \tag{21}$$

and is more favorable than the 9R structure if

$$A < \frac{32}{3}\left(\frac{U_3}{U_{32}}\right)^2 - 14. \tag{22}$$

It follows from an examination of inequalities (17), (21), and (22) that ISS-I is formed with softening of elastic moduli c' and c_{44}. Meanwhile, the value of c' should not decrease greatly with the approach of the point M_S (the parameter A should not be too large). Otherwise, restructuring by means of a single wave (k_2, e_2) would be possible (20). This situation evidently occurs in bcc alloys with a large anisotropy parameter (A >10) which undergo bcc → NR martensite transformations [38]. As regards the values of U_3/U_{31} and U_3/U_{32}, we can only assume for now that they are greater than unity.

The qualitative conclusions reached here are in accord with the earlier discussed temperature dependences of elastic moduli c_{ij} in an NiTi alloy [19]. The unusual behavior of the elastic properties (the small value of A and its decrease) account for the specific features of the instability of these alloys in the pretransformation region – the possibility of the formation of ISS-I's of a complex type describable by a combination of interacting transverse waves of atomic displacements. In other bcc alloys the determining factor is either softening of c_{44}, which facilitates the occurrence of ω-displacements (19), or intensive softening of c', which corresponds to the initial stage of Zener instability of bcc lattices in the shear systems $\{110\}\langle\bar{1}10\rangle$ [38].

2. We will briefly discuss the possibility of formation of ISS-II's, which lead to extra reflections of the "1/2" type in electron diffraction patterns and which in the representation of fluctuational atomic displacements can be described by waves with $k = \frac{1}{2}\langle 110\rangle$, $e_k \| \langle\bar{1}10\rangle$. These waves account for the main shortwave deformation of the lattice during B2 → B19' [14] and β(bcc) → α(cpu) [39] martensitic transformations. For these waves, the expansion of free energy does not contain odd powers with respect to amplitude, and a metastable structure occurs if the shortwave displacements of the atoms are accompanied by homogeneous lattice distortion. One case in which compression of a crystal along $\langle 110\rangle$ was considered was examined in [40]. In the B2 → B19' transformation, the additional homogeneous deformation is orthorhombic distortion with a small amount of monoclinic distortion (or without the latter for the B2 → B19 transformation) [14] (Fig. 12). In the $\beta \to \alpha$ transformation, homogeneous shears $\{112\}$ occur along $\langle 11\bar{1}\rangle$ [39].

Analysis of the thermodynamic stability of the initial lattice in regard to structural deformation corresponding to ISS-II can be accomplished in a manner similar to that for ISS-I (see [40]). However, it should be kept in mind [39] that, even for simple bcc metals, on the boundary of the Brillouin zone there is a minimum in the dispersion law for transverse phonons with $\mathbf{k} \| \langle 110\rangle$, $e_k \| \langle\bar{1}10\rangle$ (a similar reduction in atom vibration frequency exists near the boundary of the zone for the other branches as well: transverse with $\mathbf{k} \| \langle 111\rangle$ and longitudinal with $\mathbf{k} \| \langle 100\rangle$). Such behavior cannot be obtained within the framework of the Born–Karman theory, considering the interaction of atoms in nearest-neighbor coordination spheres and the anomaly evidently connected with long-range interactions. This points out the limitation of our method in cases when phonon anomalies are due to long-range action and structural transformations are characterized by a wave vector on the boundary of the Brillouin zone.

CONCLUSION

The unique physical properties of NiTi alloys, which are of practical importance, are governed primarily by the structural state and structural transformations dependent on temperature, chemical composition, and

processing or service conditions. However, analysis of the literature data on the premartensitic state and phase transformations in these alloys shows that until now there has been no unified physical representation of the effects observed in these systems. In connection with this, we undertook a comprehensive study of the fine structure and physical properties and their interaction in a broad range of NiTi and NiTiX (X = Fe, Cu) alloys which undergo a thermoelastic martensitic transformation in order to determine features of the change in the stability of the crystalline lattice and the structural state, as well as the sequence and structural continuity of the phase transformations and associated physicomechanical property anomalies. We also performed a thermodynamic analysis of the stability of possible pretransformation shear structures, the latter being (as follows from the empirical data) precursors of the intermediate and final martensite phases. It was established that the variety of structural changes in NiTi alloys is due to the unusual (compared to other bcc alloys) behavior of the elastic properties above the martensitic transformation point M_S. Judging from analysis of structural data, measurements of elastic moduli and electrical resistivity, and the results of theoretical study, it can be concluded that the decrease in stability of the crystalline lattice with the approach of M_S is accompanied by the realization of a sequence of genetically related structural transformations. These transformations begin with an increase in the short-range order of the atomic displacements in the initial high-temperature B2 phase. This is followed by the formation of a microdomain structure characterized by intermediate shear structures (ISS-I, ISS-II). The structure ISS-I is the precursor of the B2 → R martensitic transformation, while ISS-II precedes the formation of monoclinic B19' (or orthorhombic B19) martensite. It was shown that shear martensitic restructuring in the initial phase can be assured by reinforcement of the correlations of the periodic shortwave atomic displacements (their self-consistent, phased character), along with the necessary homogeneous deformation. When examined in this manner, the localized premartensitic displacement structures are centers of nucleation of martensite crystals.

The sequence of structural transformations in NiTi alloys can be represented in the form of the scheme:

$$B2 \rightarrow \{\text{DSO}\} \rightarrow \left\{\begin{matrix}\text{ISS -I}\\ \text{ISS -II}\end{matrix}\right\} \rightarrow \left\{\begin{matrix}R\\ B19\end{matrix}\right\} \rightarrow B19'$$

(inside the B2 phase)

LITERATURE CITED

1. L. G. Kahndros and I. A. Arbuzova, in: Metals, Electrons, Lattice [in Russian], Naukova Dumka, Kiev (1974), pp. 109-143.
2. I. I. Kornilov, O. K. Belousov, and E. V. Kachur, Titanium Nickelide and Other Alloys with the "Memory" Effect [in Russian], Nauka, Moscow (1977).
3. F. E. Wang, W. J. Buchler, and S. J. Pickart, J. Appl. Phys., 36, No. 10, 3232 (1965).
4. K. Chandra and G. R. J. Purdy, J. Appl. Phys., 39, No. 5, 2176 (1968).
5. G. D. Sandrock, A. J. Perkins, and R. F. Hehemann, Metall. Trans., 2, No. 10, 2769 (1971).
6. K. Otsuka, T. Sawamura, and K. Shimizu, Phys. Status Solidi, A, 5, No. 2, 457 (1971).
7. A. J. Nagasawa, J. Phys. Soc. Jpn., 31, No. 1, 136 (1971).
8. R. H. Bricknell, K. N. Melton, and O. Mercier, Metall. Trans., 10A, No. 6, 693; 11A, No. 9, 1541 (1980).
9. S. M. Shapiro, Metall. Trans., 12A, No. 4, 567 (1981).
10. C. M. Hwang and C. M. Wayman, Scr. Metall., 17, No. 3, 381, 385 (1983).
11. C. M. Hwang, M. Meichle, M. B. Salamon, and C. M. Wayman, Philos. Mag., 47A, No. 1, 9, 31 (1983).
12. G. R. Purdy and J. G. Parr, Trans. AIME, 221, 636 (1961).
13. M. J. Marcinkowski, A. S. Sastri, and D. Koskimaki, Philos. Mag., 18, No. 155, 945 (1968).
14. R. F. Hehemann and G. D. Sandrock, Scr. Metall., 5, No. 9, 801 (1971).
15. D. P. Dautovich and G. R. Purdy, Can. Metall. Q., 4, No. 1, 129 (1965).
16. Ch. P. Gupta, A. A. Johnson, and K. Mukherjee, Mater. Sci. Eng., 11, No. 1, 43 (1973).
17. C. M. Hwang, M. B. Salamon, and C. M. Wayman, Philos. Mag., 47A, No. 2, 177 (1983).
18. A. S. Savvinov, Author's Abstract of Candidate Dissertation, SFTI, Tomsk (1983).
19. O. Mercier, K. N. Melton, G. Gremaud, and J. J. Hägi, J. Appl. Phys., 51, No. 3, 1833 (1980).
20. V. N. Khachin, Yu. I. Paskal', et al., Fiz. Met. Metalloved., 46, No. 3, 511 (1978).
21. V. É. Gyunter, V. N. Khachin, V. P. Sivokha, and E. F. Dudarev, Fiz. Met. Metalloved., 47, No. 4, 893 (1979).
22. V. G. Pushin, V. N. Khachin, A. S. Savvinov, and V. V. Kondrat'ev, Dokl. Akad. Nauk SSSR, 227, No. 6, 1388 (1984).

23. V. N. Khachin, V. É. Gyunter, L. A. Monasevich, and Yu. I. Paskal', Dokl. Akad. Nauk SSSR, 234, No. 5, 1059 (1977).
24. D. P. Dautovich, Z. Melkvi, G. R. Purdy, and C. V. Stager, J. Appl. Phys., 37, 2513 (1966).
25. R. J. Wasilewski, S. R. Buttler, and J. E. Hanlson, Met. Sci. J., 1, No. 1, 104 (1967).
26. L. A. Monasevich, V. E. Egorushkin, Yu. I. Paskal', and V. P. Fadin, Fiz. Met. Metalloved., 50, No. 4, 803 (1980).
27. Yu. D. Tyapkin and I. V. Lyasotskii, in: Results of Science and Technology. Physical Metallurgy and Heat Treatment Series [in Russian], Vol. 15, Izd. VINITI, Moscow (1981), pp. 47-110.
28. A. W. Overhauser, Phys. Rev., 167, 691 (1968); B3, 3173 (1971).
29. M. A. Krivoglaz, Theory of Scattering of X-Rays and Thermal Neutrons by Real Crystals [in Russian], Nauka, Moscow (1967).
30. G. Honjo, S. Kodera, and N. J. Kitamura, J. Phys. Soc. Jpn., 19, No. 3, 351 (1964).
31. K. Mukherjee, M. Chandrasekaran, and F. Milillo, "Premartensite–martensite transitions related to shape memory effect," in: Shape Memory Effect Alloys, New York–London (1975), pp. 177-201.
32. P. Moine, G. M. Michal, and R. Sinclair, Acta Metall., 30, No. 1, 109, 124 (1982).
33. K. N. Melton and O. Mercier, Scr. Metall., 12, No. 1, 5 (1978).
34. O. Mercier and K. N. Melton, Metall. Trans., 10A, No. 2, 387 (1979).
35. V. V. Kondrat'ev and Yu. D. Tyapkin, in: Martensitic Transformations [in Russian], Naukova Dumka, Kiev (1978), p. 43.
36. I. I. Naumov, V. E. Panin, and M. F. Zhorovkov, Fiz. Met. Metalloved., 48, No. 1, 231 (1979).
37. V. V. Kondrat'ev, Fiz. Met. Metalloved., 41, No. 6, 1169 (1976).
38. N. Nakanishi, Prog. Mater. Sci., 24, Nos. 3-4, 142 (1979).
39. M. J. Iizumi, J. Phys. Soc. Jpn., 52, No. 2, 549 (1983).
40. V. V. Kondrat'ev, V. G. Pushin, R. R. Romanova, Yu. D. Tyapkin, and E. E. Yurchikov, Fiz. Met. Metalloved., 45, No. 4, 771 (1978).

SHAPE MEMORY EFFECTS. PROBLEMS AND PROSPECTS

V. A. Likhachev

UDC 539.319:539.219.2

INTRODUCTION

The physicomechanical properties of materials which undergo reversible martensite transformations are very unusual and varied, and they have not yet been fully investigated. Several important problems of a practical nature remain unresolved. There is no quantitative theory on shape memory effects and transformation strain. Nevertheless, continued analysis of all aspects of the problem is of course necessary for further development of representations on the properties of materials of this class and for the broad practical implementation of the results of scientific investigations. The present report discusses individual key aspects pertaining to metals and alloys exhibiting reversible martensite transformations and makes no pretense of embracing the problem as a whole. The content of this article is based on the results of studies of recent years in which the author participated and which have been reflected in conference reports and original publications [1-67]. Several of the findings discussed here and involving the author's participation are being published for the first time.

First we will enumerate the fundamental laws governing the structural-mechanical behavior of materials in connection with reversible martensite transformations (MT).

1. All metals and alloys exhibiting MT demonstrate the shape memory effect (SME), i.e., a capacity to partially or fully recover during MT strain acquired prior to the MT.

A. A. Zhdanov State University, Leningrad. Translated from Izvestiya Vysshikh Uchebnykh Zavedenii, Fizika, No. 5, pp. 22-40, May, 1985.

0038-5697/85/2805-0355$09.50